



Catalytic oxidation of benzene over Mn modified TiO₂/ZSM-5 under vacuum UV irradiation



Haibao Huang^{a,*}, Huiling Huang^a, Qiuyu Feng^a, Gaoyuan Liu^a, Yujie Zhan^a, Muyan Wu^a, Haoxian Lu^a, Yajie Shu^a, Dennis Y.C. Leung^b

^a School of Environmental Science and Engineering, Sun Yat-Sen University, China

^b Department of Mechanical Engineering, The University of Hong Kong, Pokfulam Road, Hong Kong

ARTICLE INFO

Article history:

Received 27 July 2016

Received in revised form 17 October 2016

Accepted 29 October 2016

Available online 31 October 2016

Keywords:

Mn/TiO₂/ZSM-5

Multi-functional photocatalyst

Vacuum UV irradiation

O₃ elimination and utilization

Benzene degradation

ABSTRACT

Vacuum ultraviolet (VUV) irradiation was used to improve photocatalytic degradation of gaseous benzene. A multi-functional photocatalyst of 0.1%Mn/TiO₂/ZSM-5 was developed by a modified sol-gel method for the elimination and utilization of O₃, the by-product generated from VUV irradiation. O₃ was completely removed and efficiently used to enhance catalytic oxidation of benzene via ozone-assisted catalytic oxidation (OZCO). Under VUV irradiation, benzene removal efficiency was stably kept at 100% over 0.1%Mn/TiO₂/ZSM-5, however, it was only about 50% and much O₃ was residual over commercial TiO₂ (P25). 0.1%Mn/TiO₂/ZSM-5 perfectly synergized with VUV irradiation. It provides more efficient pathways besides photocatalytic oxidation, for benzene degradation. The possible mechanism of benzene degradation over 0.1%Mn/TiO₂/ZSM-5 with VUV irradiation was proposed. This is the first report of an efficient photocatalyst with superior performance for O₃ elimination and utilization.

© 2016 Elsevier B.V. All rights reserved.

1. Introduction

In recent years, serious haze pollution frequently occurred in rapidly developing countries such as India and China. It is a great threat to the atmospheric environment and people living in these regions. Volatile organic compounds (VOCs) have been proven to be one of the vital precursors to the formation of photochemical smog and their emission should be strictly controlled [1]. Besides the atmospheric environmental risk, many VOCs, such as benzene and formaldehyde, are carcinogenic and detrimental to the public health and safety [2–4]. Photocatalytic oxidation (PCO) has raised widespread interest for the abatement of low-concentration VOCs due to its merits such as strong oxidation capability under mild reaction conditions and low cost [5,6]. However, its application is still greatly limited by low efficiency and catalyst deactivation due to recalcitrant carbonaceous intermediates on the surface of photocatalyst [7–9]. Great efforts have been made to improve its photocatalytic activity and stability by doping TiO₂ [10–12] and developing new photocatalysts [13–18] or heterostructure [14,19]. However, many of them are generally not satisfactory due to the intrinsic limitation of PCO or economical and technical infeasibil-

ity. The photocatalytic oxidation of VOCs is merely attributed to electron-hole pair and OH radicals triggered by the irradiation of photocatalysts [20–22]. It is still a big challenge to fundamentally improve its photocatalytic activity.

Vacuum ultraviolet (VUV) irradiation provides a novel and efficient way to solve the associated problems with PCO [23–27]. VUV lamps have similar structure and price to UV germicidal lamps. However, besides 254 nm UV light, about 8% of the light intensity is 185 nm UV light such that it directly generates O₃ and hydroxyl radicals, both of which are highly reactive and greatly contributes to the degradation of pollutants together with photocatalytic oxidation [28]. Our previous studies showed that toluene and benzene removal efficiency in the VUV-PCO process was more than 7 times of that in the UV-PCO process. No obvious catalytic deactivation was observed in the VUV-PCO process while UV-PCO suffered from serious catalytic deactivation [23,24]. However, much ozone was residual and brought secondary pollution in the VUV-PCO process since typical TiO₂ is generally not efficient in ozone decomposition [24,29]. O₃ needs to be eliminated before final discharge. Our previous work revealed that Mn/TiO₂ can efficiently decompose O₃ despite of its poor photocatalytic activity [23]. In the meanwhile, O₃ has strong oxidizing capacity and can be used to enhance the degradation of pollutants. It is highly desirable to develop novel photocatalysts with superior capacity for the elimination and utilization of O₃ while maintaining its photocatalytic activity. More

* Corresponding author.

E-mail address: seabao8@gmail.com (H. Huang).

recently, we successfully developed 1%Mn/ZSM-5 catalysts, which are highly active for catalytic oxidation of benzene under the help of O₃ from an O₃ generator [5,30]. The porous ZSM-5 provides high surface area not only for the dispersion of metal oxides during the preparation of catalyst but also for the strong adsorption of benzene and ozone during the reaction [31].

Herein, a novel photocatalyst of Mn/TiO₂/ZSM-5 with multi-function of elimination and utilization of O₃ was developed by a modified sol-gel method, in which TiO₂ was in-situ grown on ZSM-5. It was used in a VUV-PCO process for catalytic oxidation of VOCs. Benzene was chosen as the representative VOCs for this study since it has high toxicity and photochemical activity and is regarded as a priority hazardous pollutant. The catalytic activity of Mn/TiO₂/ZSM-5 toward benzene degradation and O₃ elimination was evaluated under VUV irradiation and compared with the reference UV lamps and catalysts. To our best knowledge, this is the first report on photocatalysts with multi-functions, which made a great breakthrough of conventional photocatalysts and enlighten us to explore their potential application.

2. Experimental details

2.1. Catalyst preparation

2.1.1. (1) synthesis of Mn/TiO₂/ZSM-5 photocatalyst

Mn/TiO₂/ZSM-5 was prepared by a modified in-situ sol-gel method via the following steps: 0.0134 g manganese acetate was dissolved in 15 ml absolute ethanol, and then 3 g ZSM-5 molecular sieves (Si/Al = 200, Nankai University) was added and mixed for 1 h. 26 ml Tetrabutyltitanate and 0.2 ml HCl solution was also added into the mixture together with 0.05 ml acetylacetone as inhibitor. A mixed solution of 2 ml deionized water and 2 ml absolute ethanol was dropped wisely into the above slurry under intensive stirring. The stirring stopped till a gelatin was formed. The gelatin was aged for 12 h, and then dried at 100 °C for 10 h. The dry powder was then calcinated at 550 °C for 5 h. Thus, 0.1%Mn/TiO₂/ZSM-5 was produced with 20% TiO₂ loading.

2.1.2. (2) synthesis of TiO₂ and TiO₂/ZSM-5

20%TiO₂/ZSM-5 was prepared similarly except without the addition of Mn source. TiO₂ was also prepared with same procedure as that of Mn/TiO₂/ZSM-5 but without the addition of Mn and ZSM-5 sources. Commercial TiO₂ (P25, Degussa) was also used without further treatment for comparison. 0.1% Mn/ZSM-5 was prepared by impregnation method, which was previously described. All catalysts were grounded, tableted, crushed and sieved to 20–40 mesh before use.

2.2. Experimental set-up

Fig. 1 shows the schematic diagram of the VUV-PCO system adopted in the present study. Catalytic oxidation of benzene was carried out in a continuous-flow fixed-bed reactor with an effective volume of about 0.5 l. It was equipped with two VUV lamps (4w, Cnlight) and a quartz tube to load photocatalyst. The 254 nm UV lamps was also tested as reference. The concentrations of benzene, and the CO and CO₂ generated from benzene oxidation were measured by gas chromatography (GC) (9790II, Fuli) equipped with two flame-ionization detectors (FID). One FID was connected with a Rt-Q-BOND PLOT column (30m × 0.25 mm id, film thickness 10μm) and used for benzene analysis. The injection and detector temperature was 100 °C and 250 °C, respectively. The other FID equipped with a packed column (TDX-01, 3m × 3 mm) followed by a methanizer was used to determine the concentrations of CO and CO₂. Gas samples from the reaction system were on-line fed to the GC by an automatic gas sampling valve. The O₃ concentration was monitored

by an ozone analyzer (202, 2 B Technology). Air, with a flow rate of 1L/min containing 25 ppm benzene and a relative humidity of 50% was introduced into the reactor. The relative humidity of 50% was found to be the optimum level in our previous study [23]. 1 g of the catalyst produced with 20–40 mesh size was used in the test, corresponding to a gas hourly space velocity (GHSV) of 60,000 ml/g_{cat} h. The VUV lamps was switched on after benzene adsorption reached equilibrium on the catalysts.

2.3. Catalyst characterization

The size and morphology of the catalysts were recorded using scanning electron microscopy (SEM) (400F, Quanta) and transmission electron microscope (TEM) (Tecnai G2 Spirit, FEI). The surface area and pore volumes were obtained from a N₂ adsorption/desorption analysis conducted at 77 K on a Micromeritics Tristar II 3020 system. The specific surface area was calculated by the BET method. The micropore and external surface area as well as the micropore volume were determined by the t-plot method. The mesopore volume was derived from the adsorption isotherm according to the Barrett-Joyner-Halenda (BJH) model. Phase structures were analyzed by XRD (Empyrean, PANalytical) using Cu K α radiation (1.5406 Å). The intensity data were collected in a 2θ range from 20° to 80°. UV-vis absorption spectra were recorded from 200–600 nm from 200 to 600 nm using a UV-vis spectrometer (UV-2501PC, Shimadzu).

3. Results and discussion

3.1. Characterization

(1) SEM and TEM images

The particle morphology of the samples was investigated using SEM. Representative SEM images are presented in Fig. 2. The unsupported TiO₂ particles appeared as agglomeration (Fig. 2a). Compared with raw ZSM-5 (Fig. 2b), it is clear that the surface of the supported samples was covered by the TiO₂ cluster, as shown in Figs. 2c and d. The cluster was slightly aggregated on TiO₂/ZSM-5 (Fig. 2c) while it got much smaller and highly dispersed on Mn/TiO₂/ZSM-5 (Fig. 2d).

To clearly observe the particle size, distribution and morphology of TiO₂, TEM operation was performed and the TEM images are shown in Fig. 3. As shown in Fig. 3a, the particle size of TiO₂ prepared by sol-gel method mainly ranged from 30 nm to 60 nm. Slight agglomeration was observed over them since the nano-TiO₂ has small particles size and high surface energy, which makes them mutual affinity and aggregation. Compared with raw ZSM-5 (Fig. 3b), it can be observed that the supported ZSM-5 was covered with highly dispersed TiO₂ particles. The TiO₂ particles grew in-situ on the surface of ZSM-5 during the preparation using the modified sol-gel method. The particle size of TiO₂ greatly reduced to 10–20 nm over TiO₂/ZSM-5 (Fig. 3c) and further decreased to 5–10 nm over the 0.1%Mn/TiO₂/ZSM-5 (Fig. 3d). The addition of Mn greatly improves the dispersion of TiO₂ particles. The fine dispersed TiO₂ particles provide more chances to be irradiated and more catalytic active sites. TiO₂ particles are mainly located on the surface of ZSM-5 rather than in the pore of ZSM-5 since the pore diameter of ZSM-5 is only about 0.5 nm [32], which is much smaller than the particle size of TiO₂ (about 10–20 nm). This small pore size of ZSM-5 prevents TiO₂ particles from penetrating into its inner pore.

(2) surface area and porosity

The textural properties of the as-prepared catalysts are listed in Table 1. The BET surface area of the unsupported TiO₂ is only 18.9 m²/g, however, it reached a high value of 373.2 m²/g over raw ZSM-5 and was dropped to 307.8 m²/g after supporting TiO₂. The

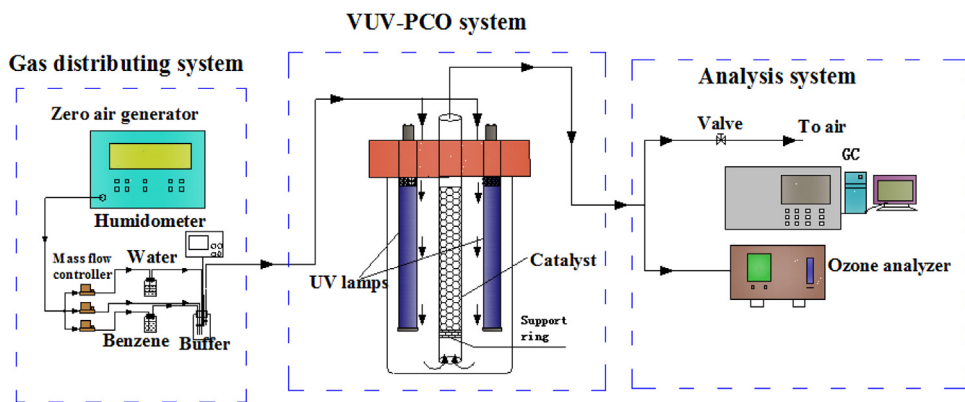


Fig. 1. The schematic diagram of VUV-PCO system.

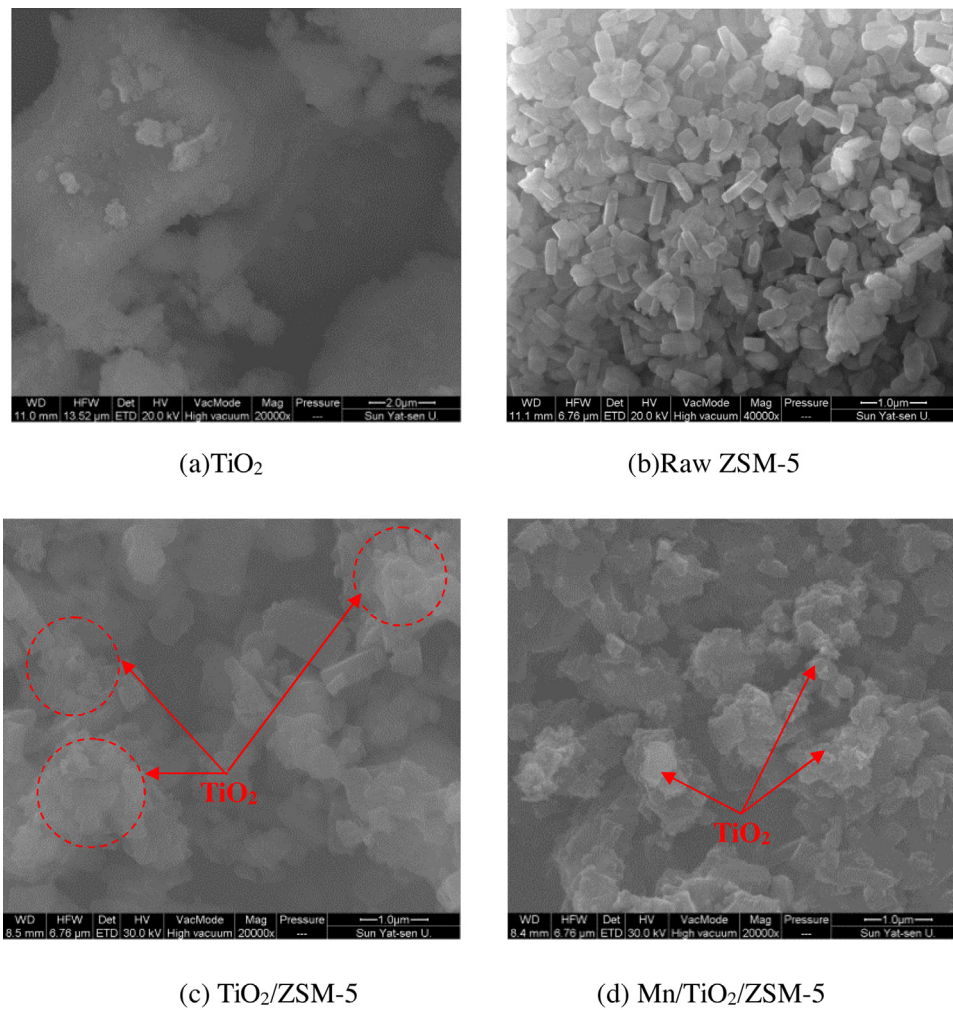
Fig. 2. SEM images of different catalysts: (a) TiO₂, (b) Raw ZSM-5, (c) TiO₂/ZSM-5, and (d) Mn/TiO₂/ZSM-5.

Table 1

Textural characteristics of the as-prepared catalysts.

Catalysts	BET surface area, m ² /g	Micropore surface area, m ² /g	External surface area, m ² /g	Pore volume (cm ³ /g)
TiO ₂	18.9	5.1	11.75	0.083
ZSM-5	373.2	257.0	116.2	0.233
TiO ₂ /ZSM-5	307.8	224.9	82.8	0.210
Mn/TiO ₂ /ZSM-5	310.3	245.6	64.8	0.199

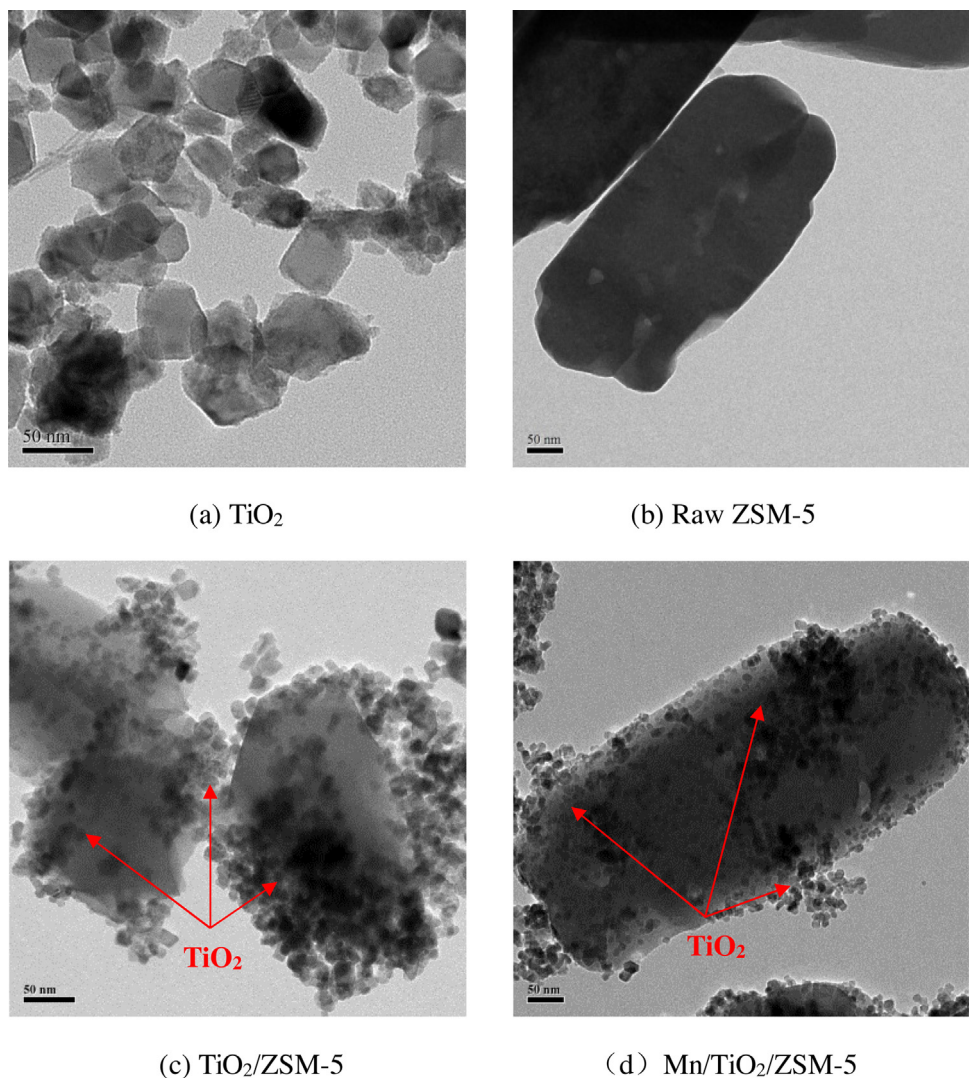


Fig. 3. TEM images of different catalysts: (a) P25, (b) TiO₂, (c) TiO₂/ZSM-5, and (d) Mn/TiO₂/ZSM-5.

high BET surface area of ZSM-5 can increase the dispersion of TiO₂ and reduce particle size, as observed in Fig. 3. After loading with TiO₂, the external surface area and pore volume of ZSM-5 decreased from 116.2 to 82.8 m²/g and from 0.233 to 0.210 cm³/g, respectively. This is due to the fact that the surface of ZSM-5 was covered by TiO₂ particles and large pores were partially blocked. Compared with TiO₂/ZSM-5, Mn/TiO₂/ZSM-5 even achieved a little higher BET and micropore surface area, further indicating that the doping of Mn can improve the dispersion of TiO₂/ZSM-5. This well agreed with the results of SEM and TEM images.

(3) XRD patterns

The XRD patterns of the as-prepared catalysts are depicted in Fig. 4. The XRD patterns of anatase TiO₂ have a main peak at $2\theta = 25.2^\circ$ corresponded to the 101 plane (JCPDS 21-1272) while the main peaks of rutile and brookite phases are at $2\theta = 27.4^\circ$ (110 plane) and $2\theta = 30.8^\circ$ (121 plane), respectively [12]. It can be found that small rutile peak appeared in the XRD pattern of P25 apart from main anatase peaks. Unlike P25, only anatase peak can be observed in the XRD pattern of TiO₂ prepared by sol-gel and its peak at 25.2° got notably sharpened and intense, demonstrating that the crystallinity got better with increased particle size were increased, which well agreed with the results of TEM images. TiO₂ also existed in its anatase phase after it was supported on ZSM-5 while the diffraction peak at 25.2° became much weaker and widened, indicating that TiO₂ particles were of small size and well dispersed on ZSM-5. This is well consistent with the results of the TEM images. The diffraction peaks of ZSM-5 were also observed over the supported TiO₂, showing that the framework structure of ZSM-5 was

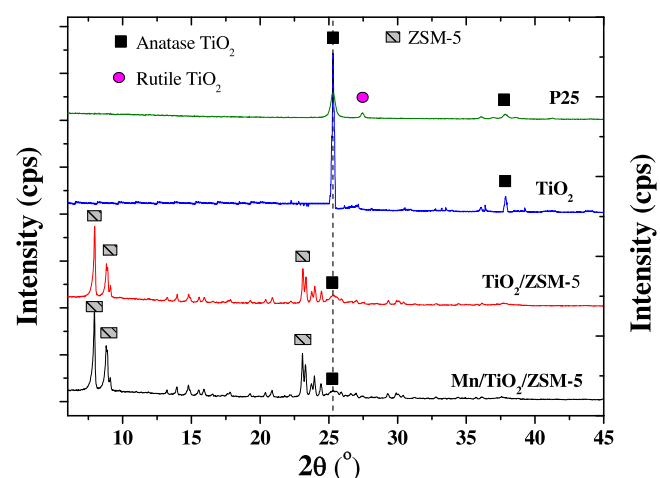


Fig. 4. XRD patterns of the as-prepared catalysts.

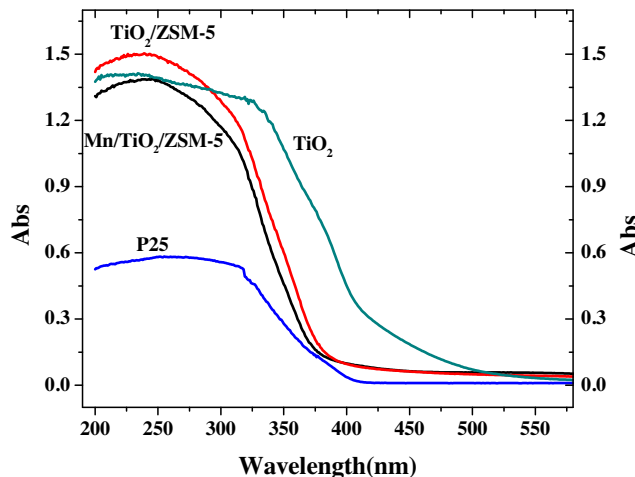


Fig. 5. UV-vis spectra of the as-prepared catalysts.

reasonably retained even after loading of TiO_2 . No obvious Mn peak was observed in the XRD patterns of the $\text{Mn}/\text{TiO}_2/\text{ZSM-5}$ due to its extremely low concentration.

(4) UV-vis absorption spectra

Fig. 5 presents the UV-vis spectra of P25, raw TiO_2 and the supported TiO_2 . It is clear that the UV absorption resulting from TiO_2 occurs in all the samples. Compared with P25, the ZSM supported TiO_2 has much stronger absorbance in the 200–400 nm region although its TiO_2 dosage is only 20% of the former, indicating that they has better absorption and utilization of UV irradiation. The absorption edges of the supported catalysts are similar and both significantly shifted to shorter wavelength regions (viz. blue shift) compared with that of the unsupported TiO_2 , as previously reported in the literature [33,34]. The absorption performance reflects the TiO_2 size difference of samples. In general, small particles tend to make blue shift [35]. This implied that the particle size of TiO_2 is greatly decreased over ZSM-5, which is consistent with the observation of the TEM images in Fig. 3. It is believed that the structure constraint effect of molecular sieve ZSM-5 can restrict the growth of TiO_2 crystal [33].

3.2. Catalytic activity evaluation

(1) photocatalytic oxidation of benzene

The photocatalytic activities of different catalysts were evaluated with 254 nm UV irradiation. Fig. 6 shows benzene removal efficiency and the concentration of CO_2 generated from benzene oxidation over different catalysts under UV irradiation. As shown in Fig. 6a, benzene removal efficiency follows the order: $\text{Mn}/\text{TiO}_2/\text{ZSM-5} \approx \text{TiO}_2/\text{ZSM-5} > \text{P25} > \text{TiO}_2 > \text{None}$. The reference samples, P25 and TiO_2 , both have poor stability towards photocatalytic oxidation of benzene. For these two photocatalysts, benzene removal efficiency quickly dropped to below 5% and eventually to nearly 0 after reaction for 3 h, indicating complete deactivation of the photocatalysts. The supported TiO_2 samples exhibited much better photocatalytic activity than the unsupported ones although its TiO_2 dosage is only 20% of the latter. Benzene removal efficiency was also decreased gradually in the initial stage while it finally kept stable at about 8%. Benzene removal is ascribed to both the adsorption and PCO. To clarify the contribution of PCO, the CO_x generated from benzene oxidation was measured. No CO was identified in the UV-PCO process, indicating that CO_2 is the only product of benzene mineralization. The outlet CO_2 concentration from the benzene oxidation over different catalysts is presented in Fig. 6b. It can be found that the outlet CO_2 concentration also quickly decreased over P25 and TiO_2 while stably kept at about 10 ppm over the supported TiO_2 . As shown in Fig. 4, after being supported on ZSM-5, TiO_2 mainly existed in anatase phase, which is active for photocatalytic oxidation [36]. As previously described, the supported TiO_2 achieved higher TiO_2 dispersion and stronger UV absorbance than the unsupported ones, which can provide more active sites and generate more oxidants for benzene oxidation over the former. This may account for the increased catalytic activity and stability over $\text{TiO}_2/\text{ZSM-5}$ and $\text{Mn}/\text{TiO}_2/\text{ZSM-5}$. In the absence of photocatalysts, benzene could not be directly destructed by the UV irradiation and no CO_2 was generated. Just like raw ZSM-5 (not shown), $\text{Mn}/\text{ZSM-5}$ exhibited no photocatalytic activity. No CO_2 was generated and benzene removal was only ascribed to the adsorption of ZSM. In addition, no O_3 was detected from the UV irradiation.

(2) benzene VUV-PCO

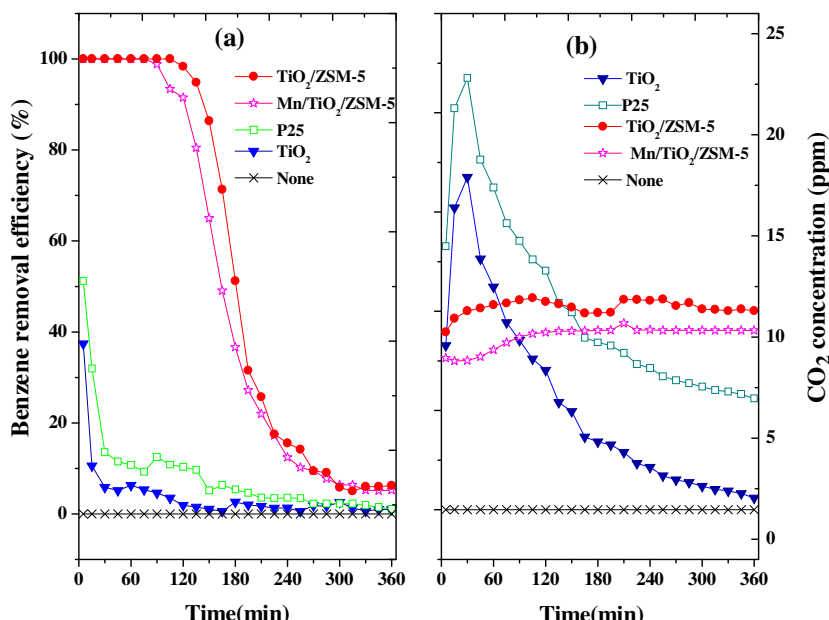


Fig. 6. Benzene removal efficiency (a), and CO_2 concentration (b) with different catalysts under UV irradiation.

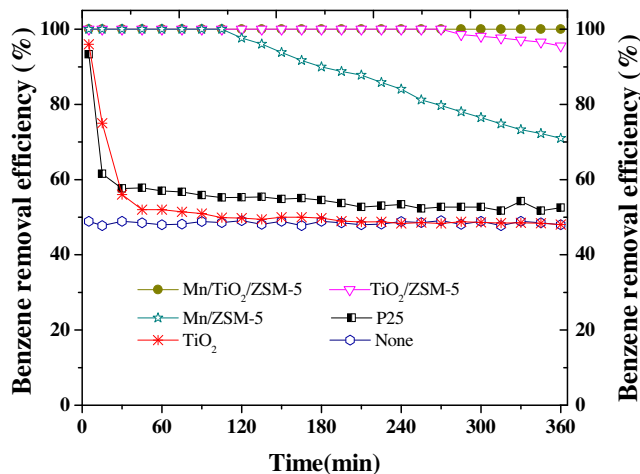


Fig. 7. Benzene removal efficiency of different catalysts under VUV irradiation.

Fig. 7 shows benzene removal efficiency of different catalysts under VUV irradiation. VUV-PCO obtained much higher benzene removal efficiency than conventional PCO. As shown in Fig. 6, benzene removal efficiency was less than 5% over typical TiO_2 and P25 under 254 nm UV irradiation and the catalysts quickly suffered from serious deactivation. However, it reached higher than 49% in all VUV irradiation process, following the order: $\text{Mn/TiO}_2/\text{ZSM-5} > \text{TiO}_2/\text{ZSM-5} > \text{Mn/ZSM-5} > \text{P25} > \text{TiO}_2 \approx \text{none}$. Benzene removal efficiency of the unsupported TiO_2 was quickly dropped to about 50%, which is close to VUV photolysis alone, demonstrating that the catalysts got easily deactivated and benzene removal is mainly ascribed to photolysis. In contrast, the benzene removal efficiency was kept 100% over $\text{TiO}_2/\text{ZSM-5}$ and dropped slightly after 270 min. Among all the samples, 0.1% $\text{Mn/TiO}_2/\text{ZSM-5}$ achieved the best catalytic activity and stability. 0.1% $\text{Mn/TiO}_2/\text{ZSM-5}$ well synergized with VUV irradiation for benzene degradation. Benzene removal efficiency was stably kept at 100%. It is even larger than the sum of that of VUV photolysis and PCO alone, indicating that more degradation pathways would be involved in benzene oxidation besides photolysis and photo-catalytic oxidation. To exclude benzene PCO, Mn/ZSM-5 was used as the catalysts for VUV irradiation. Even without TiO_2 , Mn/ZSM-5 still achieved higher benzene removal efficiency than photolysis alone, confirming the presence of more degradation pathways.

Fig. 8 shows the outlet concentration of CO_2 and CO generated from benzene degradation by different catalysts under VUV irradiation. The outlet COx concentration over various samples follows the order: $\text{Mn/TiO}_2/\text{ZSM-5} > \text{TiO}_2/\text{ZSM-5} > \text{Mn/ZSM-5} > \text{P25} > \text{TiO}_2 \approx \text{none}$, this order is the same as that of benzene removal efficiency, as shown in Fig. 7. The CO concentration of all samples are about 22 ppm, which is also close to that of photolysis alone. This suggested that CO was all formed from VUV photolysis and no CO was generated from benzene oxidation in the presence of catalysts. The CO_2 concentration slowly decreased to about 38 ppm over P25 and TiO_2 , which is close to that of VUV photolysis alone. This result further proved that benzene degradation over them is mainly ascribed to photolysis. If the contribution of VUV photolysis is excluded, the change tendency of CO_2 concentration over TiO_2 and P25 is quite similar under UV and VUV irradiation. However, the CO_2 concentration is greatly increased over the supported samples under VUV irradiation, confirming that benzene removal was attributed to oxidation but not adsorption alone. It reached 67 ppm and 85 ppm over $\text{TiO}_2/\text{ZSM-5}$ and $\text{Mn/TiO}_2/\text{ZSM-5}$, respectively. Among all the samples, 0.1% $\text{Mn/TiO}_2/\text{ZSM-5}$ achieved the highest CO_2 concentration. It synergizes quite well with VUV irradiation to mineralize benzene. Therefore, the Mn doping over $\text{TiO}_2/\text{ZSM-5}$

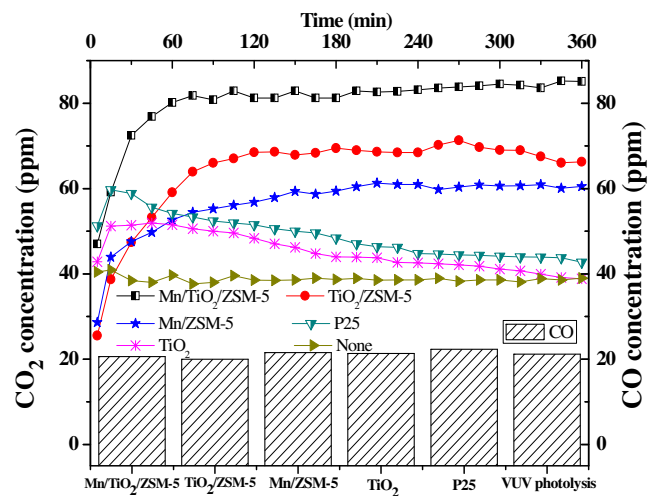


Fig. 8. Outlet COx concentration of different catalysts under VUV irradiation.

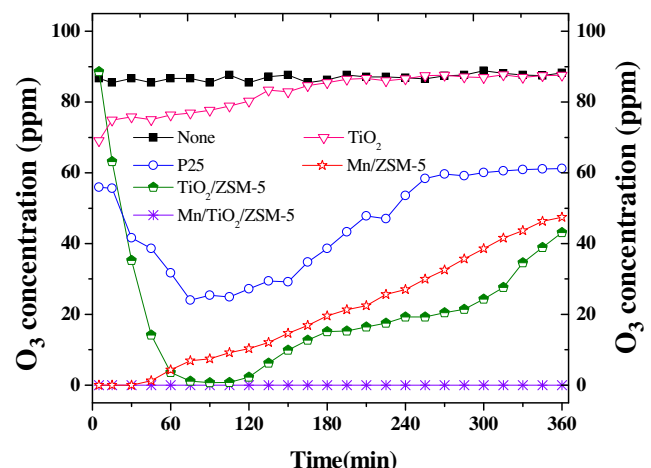


Fig. 9. Residual O_3 concentration of different catalysts under VUV irradiation.

greatly enhanced benzene degradation under VUV irradiation and Mn should be one of the active centres. Like benzene removal efficiency, its CO_2 concentration is also larger than the sum of that of VUV photolysis and PCO alone, confirming that more degradation pathways were involved in benzene oxidation besides photolysis and PCO. Without TiO_2 , Mn/ZSM-5 could also be used to catalytically oxidize benzene, as shown in Fig. 8.

In order to clarify the effect of O_3 on benzene oxidation and find out the amount of residual O_3 , the outlet O_3 concentration of different catalysts in the VUV-PCO process was measured and the results were shown in Fig. 9. In all the tests, the concentrations of O_3 generated from the VUV lamps are the same, i.e. 85 ppm. However, the residual O_3 concentrations are quite different over various catalysts, following the order: $\text{Mn/TiO}_2/\text{ZSM-5} < \text{TiO}_2/\text{ZSM-5} < \text{Mn/ZSM-5} < \text{P25} < \text{TiO}_2 \approx \text{none}$. This is just opposite to that of benzene removal efficiency and COx concentration, as shown in Figs. 7 and 8, respectively. The results implied that the decomposed O_3 was involved in the process of benzene oxidation. The residual O_3 concentration over TiO_2 quickly reached 85 ppm, which is also close to that of VUV photolysis alone. The results suggested that unsupported TiO_2 is not catalytically effective for O_3 decomposition and utilization. $\text{TiO}_2/\text{ZSM-5}$ exhibited much better catalytic activity towards O_3 decomposition while it also quickly deactivated, resulting in an increased residual O_3 concentration. Among all the samples, 0.1% $\text{Mn/TiO}_2/\text{ZSM-5}$ achieved the best cat-

alytic activity towards the decomposition and utilization of O_3 . No residual O_3 was measured in the whole test. The Mn doping over $TiO_2/ZSM-5$ greatly enhanced O_3 decomposition. Mn has been proven to be highly reactive towards catalytic decomposition of O_3 [31]. Both benzene removal efficiency and the generated COx highly depended on the capacity for O_3 catalytic decomposition. 0.1%Mn/ $TiO_2/ZSM-5$ with the best O_3 catalytic decomposition achieved the highest benzene removal efficiency and COx concentration. However, the decomposed O_3 was not always used to oxidize benzene. P25 could decompose some O_3 but benzene removal or CO_2 concentration could hardly be improved, as shown in Figs. 7 and 8. On the other hand, 0.1%Mn/ $TiO_2/ZSM-5$ well synergized with VUV irradiation to decompose O_3 and utilize it to enhance benzene degradation via ozone-assisted catalytic oxidation (OZCO). Most of the removed O_3 be used to catalytically oxidize benzene with the help of 0.1%Mn/ $TiO_2/ZSM-5$.

Therefore, among all the samples, 0.1%Mn/ $TiO_2/ZSM-5$ exhibited multi-functions under VUV irradiation and achieved the best catalytic activity in the VUV-PCO process. 100% benzene was removed, and the O_3 by-product can be completely utilized for benzene oxidation without any residual O_3 . The catalytic stability could be maintained throughout the measurement.

3.3. Scheme of benzene degradation by VUV-PCO

As indicated above, the VUV-PCO has more degradation pathways as compared with conventional PCO process. Besides PCO, VUV photolysis and OZCO are also involved during the benzene oxidation in the VUV-PCO process. They are well complement with each together so that benzene can be efficiently destructed. In the VUV-PCO process, PCO would be mainly ascribed to 254 nm UV irradiation since the emission intensity at 185 nm constitutes only 8% of all UV irradiation and it is seriously decayed in air due to the strong adsorption by O_2 and moisture [23]. As a result, very low intensity of 185 nm irradiation can be utilized to activate the TiO_2 . In the present study, PCO can roughly remove 8% of benzene and generate about 10 ppm CO_2 over $Mn/TiO_2/ZSM-5$ in the VUV-PCO process. It is generally regarded that $\cdot OH$ generated from the UV irradiation of TiO_2 is responsible for VOCs PCO [21]. VUV photolysis made a great contribution to benzene degradation. It can remove 49% benzene and generate 61 ppm CO_2 . Under VUV irradiation, hydroxyl radical ($\cdot OH$) and oxygen species such as $O(^1D)$, $O(^3P)$ and O_3 are produced via the following steps [37–39]:

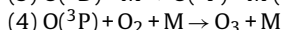
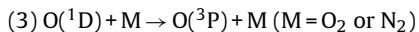
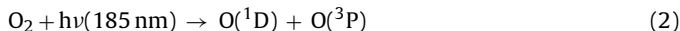
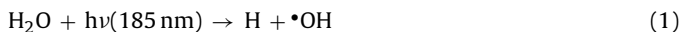
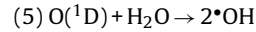


Table 2

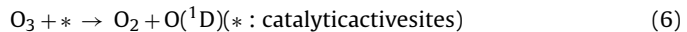
Contribution of various sub-processes to benzene removal and the COx products over $Mn/TiO_2/ZSM-5$ under VUV irradiation.

Pathways	Benzene removal efficiency, %	COx products, %
VUV-PCO	100	100
PCO	8	9
VUV photolysis	49	58
OZCO ^a	43	33

^a $OZCO \approx (VUV-PCO)-(VUV)-(PCO)$.



O_3 from VUV irradiation will be decomposed under the help of Mn catalyst, generating $O(^1D)$ and $\cdot OH$ via the following steps [5,40]:



$O(^1D)$ and $\cdot OH$ are highly reactive and can efficiently enhance benzene oxidation. Thus, $Mn/TiO_2/ZSM-5$ can simultaneously achieve elimination and utilization of O_3 through OZCO. The contribution of OZCO can be roughly calculated from the benzene removal efficiency or COx products of VUV-PCO subtracted by the contribution of VUV photolysis and PCO. It was estimated that 43% of benzene was removed by OZCO, generating 34.8 ppm CO_2 . The contribution of various sub-processes to benzene removal and COx products are summarized in Table 2.

The possible schematic of benzene oxidation in the VUV-PCO process over $Mn/TiO_2/ZSM-5$ catalyst is proposed in Fig. 10. 0.1%Mn/ $TiO_2/ZSM-5$ perfectly works with VUV photolysis to provide more pathways for synergistic benzene degradation, leading to the extremely high benzene removal efficiency and catalytic stability. Besides direct photo-oxidation, VUV lamps provide UV sources for PCO and generate O_3 for OZCO. 0.1%Mn/ $TiO_2/ZSM-5$ exhibited multi-functions under VUV irradiation. It not only triggered PCO but also decomposed and utilized O_3 to enhance benzene oxidation. ZSM-5 alone contributed little to benzene oxidation and O_3 decomposition while it has high BET surface area and appropriate pore diameter, resulting in strong capacity for benzene adsorption and prolonged reaction time [5]. The high surface area and pores can serve as reservoirs to contain the intermediate species and the residual ozone by holding them in the adsorbed phase [41]. In the meanwhile, the Lewis acid sites of ZSM-5 played a key role in ozone decomposition [42,43]. Silva et al. [44] also believed that the framework structure, textural and acidity properties of ZSM-5 contributed to the high catalytic activity and selectivity. TiO_2 acted as the active center for benzene PCO. PCO should be also involved in catalytic decomposition of O_3 since the introduction of TiO_2 into

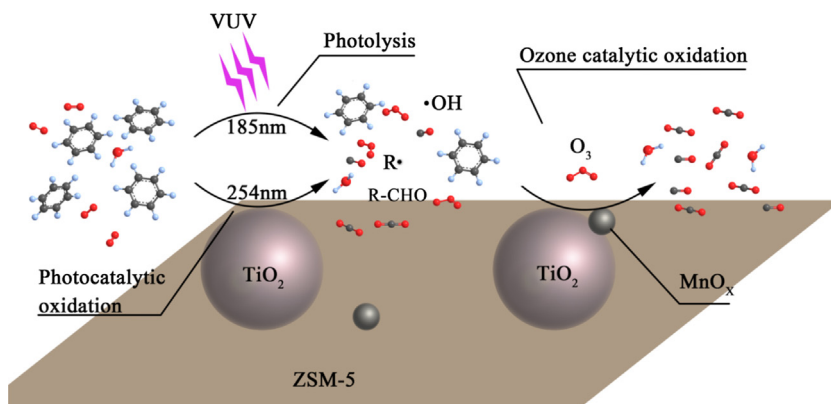


Fig. 10. The schematic of benzene oxidation in VUV-PCO process over $Mn/TiO_2/ZSM-5$ catalyst.

Mn/ZSM-5 significantly improved O₃ decomposition, as shown in Fig. 9. Mn played an important role in the multi-functional photocatalyst of Mn/TiO₂/ZSM-5. Besides increasing TiO₂ dispersion, Mn acted as the active center for catalytic decomposition of O₃ and benzene OZCO. Compared with the samples without Mn doping, the doped catalysts achieved much better catalytic activity towards benzene oxidation and O₃ decomposition. Thus, ZSM-5, TiO₂, and Mn well cooperate together to achieve multi-functions for the efficient degradation of benzene as well as elimination and utilization of O₃ under VUV irradiation.

4. Conclusions

A multi-functional photocatalyst of Mn/TiO₂/ZSM-5 was developed by a modified sol-gel method and used for benzene degradation under VUV irradiation. Both benzene and O₃ generated from VUV irradiation was completely removed over 0.1%Mn/TiO₂/ZSM-5 while benzene removal efficiency was only about 50% and much O₃ was residual over commercial TiO₂ (P25). 0.1%Mn/TiO₂/ZSM-5 perfectly synergized with VUV irradiation for benzene degradation, leading to the extremely high benzene removal efficiency and catalytic stability. It provides more efficient pathways besides photocatalytic oxidation, for benzene degradation. O₃ was transformed to active species of O(¹D) and •OH by Mn/TiO₂/ZSM-5, enhancing benzene removal of via OZCO. The scheme of benzene degradation by VUV-PCO was proposed. To our best knowledge, this is the first report of a highly efficient photocatalyst with superior performance for O₃ elimination and utilization. This study also provides a novel way to improve catalytic activity and stability of PCO.

Acknowledgment.

The authors gratefully acknowledge the financial supports from National Key Research and Development Program (No. 2016YFC0204800), NSFC-RGC (No. 51561165015, No. N_HKU718/15), Guangdong Applied Science and Technology Research & Development Fund(2015B020236004), Guangdong Special Fund for Science and Technology Development (Hong Kong Technology Cooperation Funding Scheme) (No. 2016A050503022), Science and Technology Project in Guangzhou (No. 2014Y2-00094), and the Key Fundamental Research Fund for the Central Universities (15lgjc07).

References

- R.-J. Huang, Y. Zhang, C. Bozzetti, K.-F. Ho, J.-J. Cao, Y. Han, K.R. Daellenbach, J.G. Slowik, S.M. Platt, F. Canonaco, High secondary aerosol contribution to particulate pollution during haze events in China, *Nature* 514 (7521) (2014) 218–222.
- T.-D. Pham, B.-K. Lee, C.-H. Lee, The advanced removal of benzene from aerosols by photocatalytic oxidation and adsorption of Cu-TiO₂/PU under visible light irradiation, *Appl. Catal. B: Environ.* 182 (2016) 172–183.
- X. Wang, Q. Ni, D. Zeng, G. Liao, C. Xie, Charge separation in branched TiO₂ nanorod array homojunction aroused by quantum effect for enhanced photocatalytic decomposition of gaseous benzene, *Appl. Surf. Sci.* 389 (2016) 165–172.
- H. Huang, H. Lu, Y. Zhan, G. Liu, Q. Feng, H. Huang, M. Wu, X. Ye, VUV photo-oxidation of gaseous benzene combined with ozone-assisted catalytic oxidation: effect on transition metal catalyst, *Appl. Surf. Sci.* 10.1016/j.apsusc.2016.07.040.
- H. Huang, H. Huang, Y. Zhan, G. Liu, X. Wang, H. Lu, L. Xiao, Q. Feng, D.Y. Leung, Efficient degradation of gaseous benzene by VUV photolysis combined with ozone-assisted catalytic oxidation: performance and mechanism, *Appl. Catal. B: Environ.* 186 (2016) 62–68.
- T. Yan, J. Long, X. Shi, D. Wang, Z. Li, X. Wang, Efficient photocatalytic degradation of volatile organic compounds by porous indium hydroxide nanocrystals, *Environ. Sci. Technol.* 44 (4) (2010) 1380–1385.
- J. Mo, Y. Zhang, Q. Xu, Y. Zhu, J.J. Lamson, R. Zhao, Determination and risk assessment of by-products resulting from photocatalytic oxidation of toluene, *Appl. Catal. B: Environ.* 89 (3–4) (2009) 570–576.
- H. Huang, W. Li, Destruction of toluene by ozone-enhanced photocatalysis: performance and mechanism, *Appl. Catal. B: Environ.* 102 (3–4) (2011) 449–453.
- M.D. Hernández-Alonso, F. Fresno, S. Suárez, J.M. Coronado, Development of alternative photocatalysts to TiO₂: challenges and opportunities, *Energy Environ. Sci.* 2 (12) (2009) 1231–1257.
- H. Huang, D. Li, Q. Lin, W. Zhang, Y. Shao, Y. Chen, M. Sun, X. Fu, Efficient degradation of benzene over LaVO₄/TiO₂ nanocrystalline heterojunction photocatalyst under visible light irradiation, *Environ. Sci. Technol.* 43 (11) (2009) 4164–4168.
- H. Einaga, T. Ibusuki, S. Futamura, Improvement of catalyst durability by deposition of Rh on TiO₂ in photooxidation of aromatic compounds, *Environ. Sci. Technol.* 38 (1) (2003) 285–289.
- J.B. Zhong, Y. Lu, W.D. Jiang, Q.M. Meng, X.Y. He, J.Z. Li, Y.Q. Chen, Characterization and photocatalytic property of Pd/TiO₂ with the oxidation of gaseous benzene, *J. Hazard. Mater.* 168 (2–3) (2009) 1632–1635.
- Z. Li, Z. Xie, Y. Zhang, L. Wu, X. Wang, X. Fu, Wide band gap p-block metal oxyhydroxide InOOH: a new durable photocatalyst for benzene degradation, *J. Phys. Chem. C* 111 (49) (2007) 18348–18352.
- D. Wang, Z.N. Guo, Y. Peng, W.X. Yuan, A simple route to significant enhancement of photocatalytic water oxidation on BiVO₄ by heterojunction with SiC, *Chem. Eng. J.* 281 (2015) 102–108.
- H. Wang, Y. Su, H.X. Zhao, H.T. Yu, S. Chen, Y.B. Zhang, X. Quan, Photocatalytic oxidation of aqueous ammonia using atomic single layer graphitic-C₃N₄, *Environ. Sci. Technol.* 48 (20) (2014) 11984–11990.
- J. Yu, M. Jaroniec, Preface: graphene and C₃N₄-based photocatalysts, *Appl. Surf. Sci.* 358 (Part A) (2015) 1.
- D. Huang, X. Fu, J. Long, X. Jiang, L. Chang, S. Meng, S. Chen, Hydrothermal synthesis of MSn(OH)₆ (M = Co, Cu, Fe, Mg, Mn, Zn) and their photocatalytic activity for the destruction of gaseous benzene, *Chem. Eng. J.* 269 (2015) 168–179.
- L. Ren, M. Mao, Y. Li, L. Lan, Z. Zhang, X. Zhao, Novel photothermocatalytic synergistic effect leads to high catalytic activity and excellent durability of anatase TiO₂ nanosheets with dominant {001} facets for benzene abatement, *Appl. Catal. B: Environ.* 198 (2016) 303–310.
- T. Zhang, X.L. Yan, D.D. Sun, Hierarchically multifunctional K-OMS-2/TiO₂/Fe₃O₄ heterojunctions for the photocatalytic oxidation of humic acid under solar light irradiation, *J. Hazard. Mater.* 243 (2012) 302–310.
- V. Maurino, M. Minella, F. Sordello, C. Minero, A proof of the direct hole transfer in photocatalysis: the case of melamine, *Appl. Catal. A: Gen.* 521 (2016) 57–67.
- C. Yang, Q. Li, L. Tang, K. Xin, A. Bai, Y. Yu, Synthesis, photocatalytic activity, and photogenerated hydroxyl radicals of monodisperse colloidal ZnO nanospheres, *Appl. Surf. Sci.* 357 (Part B) (2015) 1928–1938.
- S. Wang, L. Pan, J.-J. Song, W. Mi, J.-J. Zou, L. Wang, X. Zhang, Titanium-defected undoped anatase TiO₂ with p-Type conductivity room-temperature ferromagnetism, and remarkable photocatalytic performance, *J. Am. Chem. Soc.* 137 (8) (2015) 2975–2983.
- H. Huang, H. Huang, L. Zhang, P. Hu, X. Ye, D.Y. Leung, Enhanced Degradation of gaseous benzene under vacuum ultraviolet (VUV) irradiation over TiO₂ modified by transition metals, *Chem. Eng. J.* 259 (2015) 534–541.
- H. Huang, D.Y.C. Leung, G. Li, M.K.H. Leung, X. Fu, Photocatalytic destruction of air pollutants with vacuum ultraviolet (VUV) irradiation, *Catal. Today* 175 (1) (2011) 310–315.
- P. Fu, Characterization of Pt-TiO₂ film used in three formaldehyde photocatalytic degradation systems UV₂₅₄ nm, O₃ + UV₂₅₄ nm and UV₂₅₄₊₁₈₅ nm via X-ray photoelectron spectroscopy, *Chin. J. Catal.* 35 (2014) 210–218.
- P.Y. Zhang, J. Liu, Z.L. Zhang, VUV photocatalytic degradation of toluene in the gas phase, *Chem. Lett.* 33 (10) (2004) 1242–1243.
- M. Sayed, P. Fu, L.A. Shah, H.M. Khan, J. Nisar, M. Ismail, P. Zhang, VUV-Photocatalytic degradation of bezafibrate by hydrothermally synthesized enhanced {001}facets TiO₂/Ti film, *J. Phys. Chem. A* 120 (1) (2016) 118–127.
- K. Zoschke, H. Bornick, E. Worch, Vacuum-UV radiation at 185 nm in water treatment—a review, *Water Res.* 52 (2014) 131–145.
- J. Jeong, K. Sekiguchi, K. Sakamoto, Photochemical and photocatalytic degradation of gaseous toluene using short-wavelength UV irradiation with TiO₂ catalyst: comparison of three UV sources, *Chemosphere* 57 (7) (2004) 663–671.
- H. Huang, X. Ye, W. Huang, J. Chen, Y. Xu, M. Wu, Q. Shao, Z. Peng, G. Ou, J. Shi, Ozone-catalytic oxidation of gaseous benzene over MnO₂/ZSM-5 at ambient temperature: catalytic deactivation and its suppression, *Chem. Eng. J.* 264 (2015) 24–31.
- H. Huang, W. Huang, Y. Xu, X. Ye, M. Wu, Q. Shao, G. Ou, Z. Peng, J. Shi, J. Chen, Q. Feng, Y. Zan, H. Huang, P. Hu, Catalytic oxidation of gaseous benzene with ozone over zeolite-supported metal oxide nanoparticles at room temperature, *Catal. Today* 258 (2015) 627–633.
- W. Zhang, F. Bi, Y. Yu, H. He, Phosphoric acid treating of ZSM-5 zeolite for the enhanced photocatalytic activity of TiO₂/HZSM-5, *J. Mol. Catal. A: Chem.* 372 (2013) 6–12.
- J. Yuan, X. Huang, M. Chen, J. Shi, W. Shangguan, Ozone-assisted photocatalytic degradation of gaseous acetaldehyde on TiO₂/M-ZSM-5 (M = Zn, Cu, Mn), *Catal. Today* 201 (2013) 182–188.
- A.N. Ökte, Yılmaz Ö, Characteristics of lanthanum loaded TiO₂-ZSM-5 photocatalysts: decolorization and degradation processes of methyl orange, *Appl. Catal. A: Gen.* 354 (1–2) (2009) 132–142.

- [35] Y. Al-Douri, K.D. Verma, D. Prakash, Optical investigations of blue shift in ZnS quantum dots, *Superlattices Microstruct.* 88 (2015) 662–667.
- [36] W. Li, Y. Bai, C. Liu, Z. Yang, X. Feng, X. Lu, N.K. van der Laak, K.-Y. Chan, Highly thermal stable and highly crystalline anatase TiO₂ for photocatalysis, *Environ. Sci. Technol.* 43 (14) (2009) 5423–5428.
- [37] P. Bergonzo, I.W. Boyd, Low pressure photodeposition of silicon nitride films using a xenon excimer lamp, *Appl. Phys. Lett.* 63 (13) (1993) 1757–1759.
- [38] T. Hashem, M. Zirlewagen, A. Braun, Simultaneous photochemical generation of ozone in the gas phase and photolysis of aqueous reaction systems using one VUV light source. a, *Water Sci. Technol.* 35 (4) (1997) 41–48.
- [39] P. Fu, Photocatalytic degradation of low concentration formaldehyde and simultaneous elimination of ozone by-product using palladium modified TiO₂ films under UV_{254+185nm} irradiation, *Appl. Catal. B: Environ.* 105 (2011) 220–228.
- [40] H. Einaga, Y. Teraoka, A. Ogata, Catalytic oxidation of benzene by ozone over manganese oxides supported on USY zeolite, *J. Catal.* 305 (2013) 227–237.
- [41] C.W. Kwong, C.Y. Chao, K. Hui, M. Wan, Catalytic ozonation of toluene using zeolite and MCM-41 materials, *Environ. Sci. Technol.* 42 (22) (2008) 8504–8509.
- [42] S. Alejandro, H. Valdes, C. Zaror, Natural zeolite reactivity towards ozone: the role of acid surface sites, *J. Adv. Oxid. Technol.* 14 (2) (2011) 182–189.
- [43] N. Brodu, M.-H. Manero, C. Andriantsiferana, J.-S. Pic, H. Valdés, Role of Lewis acid sites of ZSM-5 zeolite on gaseous ozone abatement, *Chem. Eng. J.* 231 (2013) 281–286.
- [44] B. Silva, H. Figueiredo, O.S.G.P. Soares, M.F.R. Pereira, J.L. Figueiredo, A.E. Lewandowska, M.A. Bañares, I.C. Neves, T. Tavares, Evaluation of ion exchange-modified Y and ZSM-5 zeolites in Cr(VI) biosorption and catalytic oxidation of ethyl acetate, *Appl. Catal. B: Environ.* 117–118 (2012) 406–413.